Optimisation of a polygon mirror-based spectral filter for swept source optical coherence tomography (SS-OCT)

Michael Everson, Virgil-Florin Duma, George Dobre

Michael Everson, Virgil-Florin Duma, George Dobre, "Optimisation of a polygon mirror-based spectral filter for swept source optical coherence tomography (SS-OCT)," Proc. SPIE 10591, 2nd Canterbury Conference on OCT with Emphasis on Broadband Optical Sources, 105910V (5 March 2018); doi: 10.1117/12.2283034

SPIE.

Event: Second Canterbury Conference on Optical Coherence Tomography, 2017, Canterbury, United Kingdom

Optimisation of a polygon mirror-based, spectral filter for Swept Source Optical Coherence Tomography (SS-OCT)

Michael Everson[1,*] Virgil-Florin Duma[2,3], George Dobre[1]

[1] Applied Optics Group, School of Physical Sciences, University of Kent, Canterbury, CT2 7NH, United Kingdom

[2] 3OM Optomechatronics Group, "Aurel Vlaicu" University of Arad, 77 Revolutiei Ave, Arad 310130, Romania

[3] Doctoral School, Polytechnic University of Timisoara, 1 Mihai Viteazu Ave, Timisoara 300222, Romania

ABSTRACT

Medical imaging using Optical Coherence Tomography (OCT) provides clinicians with 3D, high resolution reconstructions of microscopic structures, in depth. It has been initially developed for ophthalmology, in order to scan the retinas of patients to diagnose illness. The quality of the images depends upon their axial and lateral resolutions and the properties of the light being used.

Research using a polygon mirror (PM) as a spectral filter in Swept Source OCT (SS-OCT) has resulted in a variety of different experimental arrangements. Although the application of PM-based SS-OCT sources has been successfully demonstrated, the combination of their components' fundamental properties and the overall impact they have on imaging performance is rarely reported. A more detailed examination of these properties would lead to a full description of their operation and to the best methods to employ if system performance is to be maximised. This work presents our current findings of on-going research into the optimisation of PM-based SS-OCT systems.

A swept source spectral filter, consisting of a collimator, a transmission grating, a two-lens telescope and an off-axis PM with an end reflector mirror has been evaluated experimentally and compared with theoretical predictions. The system's performance has been compared for two different fibre collimators. Although the beam width on the grating is different for each of the two collimators, the spot size at the PM facet is made the same by selecting appropriate focal lengths. An improvement in the signal roll-off at the interferometer output of ~1.0 dB/mm was obtained when using a 3.4 mm collimator compared to a 1.5 mm collimator.

Keywords: optical coherence tomography (OCT), spectral filter, polygon mirror (PM), spectral tuning, wavelength sampling, swept source (SS).

1. INTRODUCTION

Mechanically-swept sources (SSs), utilizing a multi-faceted, rotational polygon mirror (PM), provide an alternative filtering method to Micro-Electro-Mechanical Systems (MEMS)-based SSs, that has proven applications in Optical Coherence Tomography (OCT)[1-4]. Their success relies upon the filter's ability to tune fine instantaneous linewidths from a broadband spectrum in a short period of time. A number of publications have successfully demonstrated their proof of concept in a variety of creative techniques[5-7], yet few have explored, in detail, the factors that govern their overall performance or which methods will produce the best results for OCT.

PM-based filters generating at their output light in a swept narrow band can be designed to achieve this in a variety of ways, which makes them very versatile. Although state-of-the-art swept sources (SS) are capable of producing MHz scanning frequencies[8], they are typically limited by their operating wavelength[2]. A PM can operate at any wavelength and can achieve facet repetition rates of >100 kHz. This is low by comparison but still high enough to offer an

*mje23@kent.ac.uk; phone 01227 82 3288; aogkent.uk

2nd Canterbury Conference on OCT with Emphasis on Broadband Optical Sources, edited by Adrian Podoleanu, Ole Bang, Proc. of SPIE Vol. 10591, 105910V
 · doi: 10.1117/12.2283034

appreciable tuning speed for most laboratory experiments, however with techniques such as buffering, the speed can be increased further[9].

Operation at different wavelengths can be achieved at a reduced cost because the same PM can be used and multiple SSs can even be constructed to operate simultaneously[10]. One significant drawback can be the overall physical size of the spectral filter, which is substantially determined by the size of the optics and the length of the telescope, although commercial PM-based SS do exist.

High axial resolution and high depth penetration depend upon controlling the bandwidth and linewidth respectively. If either of these is not optimised in the setup, the image quality will be reduced. Due to the wide variety of different experimental arrangements that can be constructed, often little or no consideration is given to the method that guarantees the entire bandwidth is being utilised or that the linewidths are as narrow as theoretically possible.

Examination of the components properties and of the geometry of their arrangement leads to a better understanding of their physical limitations and how they may affect the bandwidth and linewidth. Therefore, it is necessary to explore both experimentally and theoretically to achieve optimum performance. The width of the beam at the PM facet in particular has an effect on the interferometric signal detected in this coherence imaging system. A secondary consideration is to attempt to maintain a small overall footprint to ensure easier and convenient transportation and operation.

2. METHODS

Our spectral filter consists of the following components: collimator, transmission grating, two-lens telescope, PM, and end reflector mirror (Fig. 1). 1300 nm broadband optical radiation is generated in a semiconductor optical amplifier, then circulated via optical fibre towards the free space filter. A collimator directs the light onto the grating, which spatially distributes the spectrum over a fixed angular displacement into the working space of Lens 1. The two-lens telescope captures and directs the collimated, narrow linewidth beams onto the facets of the PM where they are then reflected onto the end mirror.

The PM is positioned off-axis by introducing a certain eccentricity, E. This allows the converging angle at the focal plane of Lens 2 to be increased, spreading the spectrum over a larger angular displacement and therefore improving the linewidths[11]. As the PM rotates, the facet sweeps through the spectrum, reflecting the linewidths, in sequence, off the end mirror. At any instant during the sweep, only those wavelengths reflecting off the end mirror at normal incidence will make it back through the setup exactly along the same path they came and be collected by the collimator. Some of the other wavelengths will be reflected back through the telescope but they will not strike the grating at the correct angle and therefore will not be injected back into the fibre.

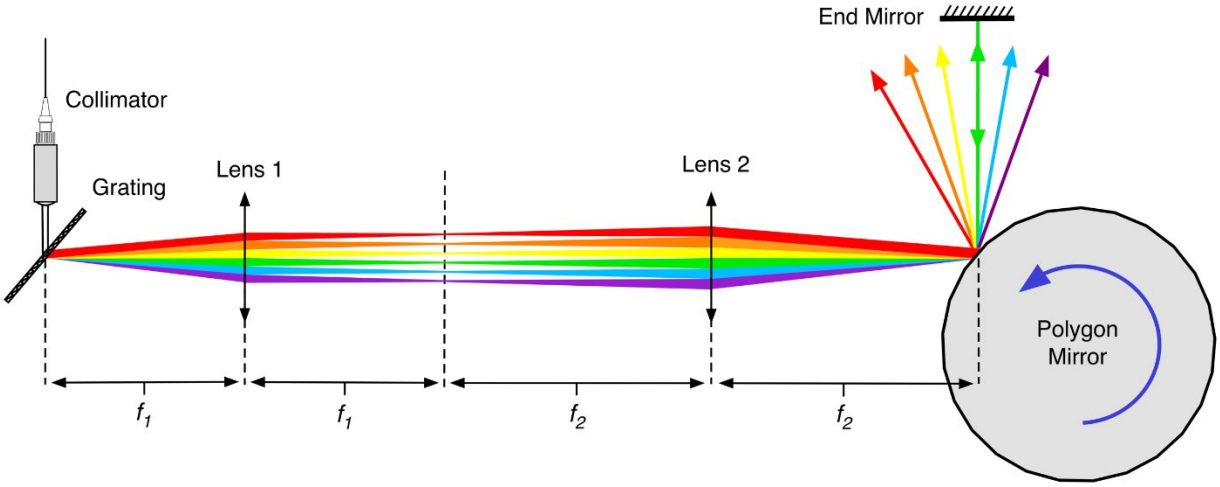

Figure 1. The spectral filter consisting of a fibre collimator, transmission grating, two lens telescope with focal lengths f_1 and f_2, PM and an end reflector mirror. As the facet sweeps through the spectrum, only those wavelengths of light at normal incidence (green trace) on the end mirror will reflect exactly along the same path to be captured by the collimator and reinjected back into the fibre.

A simple investigation of the systems performance can be carried out by changing the properties of three components; the collimators' beam diameter, the focal lengths of the telescope (f_1 & f_2), and the grating's pitch. However, for the present investigation the grating will remain unchanged. The gratings' pitch determines the maximum angular displacement, into the object space of Lens 1, between the marginal wavelengths at the edges of the spectrum. A higher line density will spread the spectrum over a larger angular range, which is preferable in order to maximize the converging angle from Lens 2 and achieve finer tuning; however this ultimately depends upon the focal lengths of the telescope. The diffraction angles for each wavelength are calculated using the grating equation:

$$\delta_n = \sin^{-1}(Gm\lambda_n - \sin\gamma) \tag{1}$$

where δ_n is the diffracted angle of a specific wavelength measured from the normal, G is the grating pitch (lines/mm), m is the diffraction order (m = 1), λ_n is the wavelength, and γ is the incident grazing angle ($\gamma = 48°$). For light with wavelengths between 1280 nm and 1390 nm (a 110 nm bandwidth), an 1145 lines/mm pitch spreads the spectrum over an angular displacement of 11.78° in the object space of Lens 1. This numerical aperture (NA_1) is found using the angle $\delta_{max} - \delta_{min}$ given by Eq. (1) and is maintained constant throughout the experiment.

The collimator produces a beam with an initial width W_0. The beam's width changes when it interacts with the grating, producing W_1, which is a function of the wavelength and is a consequence of the geometry of the alignment. In our arrangement, we find that a longer wavelength beam becomes narrower, while a shorter wavelength beam will become wider. The beam width will change again if the focal lengths f_1 and f_2 in the telescope are different. The final beam width W_2 on the facet will be a function of all of these parameters.

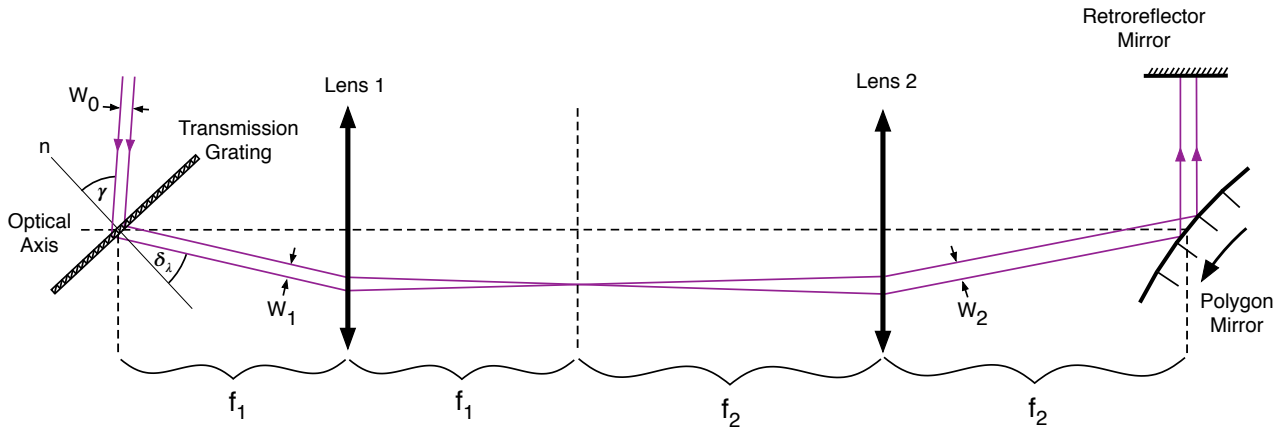

Figure 2. Diagram of the spectral filter operating at the shortest wavelength only. The initial beam width W_0 increases to W_1 by travelling through the grating. It then changes again depending on the focal lengths of Lens 1 & 2, either increasing or decreasing in size. By a careful selection of the focal lengths we can ensure that the facet will fully accommodate the final width of the beam and limit the amount of unnecessary vignetting.

Multiple telescope designs, using a different collimator and different lenses, were considered for experimental comparison. The resulting theoretical values for W_2 varied between the different designs. However, some designs resulted in W_2 values that were identical or very close (to within 2%). This makes it possible to compare two different collimators with different initial beam widths, while maintaining the same spot size on the facets of the PM. The key difference has been the focal lengths of the telescope, which has a direct impact on the overall footprint size of the setup.

A number of constraints need to be considered when selecting the lens combinations for each collimator. The size of a single facet is fixed and will restrict the maximum value of the beam width that can be effectively used on it. Any beam width larger than the size of a facet leads to losses, since this would introduce vignetting[13], and therefore should not be used. Also, the widest beam originating from the grating should be considered when calculating the final beam width on the facets. This occurs for the shortest wavelength ($\lambda_{min} = 1280\ nm$) as described above (Fig. 2). The beam width W_1 exiting the grating is given by:

$$W_1 = W_0 \frac{\cos \delta_{min}}{\cos \gamma} \tag{2}$$

where δ_{min} is given by Eq. (1), using λ_{min} for the shortest wavelength. W_2 is found by substituting the relationship between the ratios of the beam widths and the focal lengths of the telescope, $W_2 = W_1 f_2/f_1$.

$$W_2(\lambda_{min}) = W_0 \frac{\cos(\sin^{-1}(Gm\lambda_{min} - \sin\gamma))}{\cos\gamma} \cdot \frac{f_2}{f_1} \tag{3}$$

This provides the first approximation of the incident beam width W_2 on the PM facets as a function of the shortest wavelength. To achieve a more accurate value, one should consider the effect of the marginal rays passing through the lenses at angles less than normal incidence and therefore undergoing refraction. The geometry of this arrangement will contribute to a change in beam width, which will be a function of the focal lengths of the lenses, however since the angles are very small their effect can be considered negligible by comparison.

The width of a single facet *a* on the PM is given by $2R\sin(\pi/n)$, where *R* is the radius of the PM and *n* is the number of facets. We use a Lincoln Laser SA34 with 72 facets and a radius of 31.75 mm. This gives a facet width of 2.77 mm. However, the added PM eccentricity, *E*, affects the visible facet width as seen by the incident beams. Consider the central wavelength propagating along the optical axis. The facet will have rotated clockwise away from normal incidence and the visible facet width l_v will have reduced to the value $\sin\theta$, where $\theta = \cos^{-1}(E/R)$. Our PM has an eccentricity of approximately 10 mm, reducing the visible facet width to 2.63 mm. Any beam widths calculated for W_2 that are larger than this value can be considered too large and have therefore been discarded.

3. RESULTS AND DISCUSSION

Two collimators were selected for comparison; Thorlabs F240APC-C ($\emptyset = 1.5$ mm) and F280APC-C ($\emptyset = 3.4$ mm). A range of 1 inch diameter lenses with six different focal lengths (35 mm, 40 mm, 60 mm, 75 mm, 100 mm & 150 mm) were chosen and the beam widths at the facet for all the combinations were calculated, taking into consideration all the constraints discussed above. Out of 72 possible lens combinations (36 for each collimator) only 37 had beam widths smaller than the size of a visible facet (24 combinations for the first collimator (1.5 mm) and 13 for the second collimator (3.4 mm)). However, out of those 37, only 7 had beam widths for both collimators that were approximately the same size. The pairing selection process allowed for up to ± 30 μm differences between the two beam widths (~2% for the 1.5 mm beam width).

One of the secondary goals of this project is to minimise the overall footprint size of the setup, hence we excluded lens pairs that exceeded a particular total length. For example, two 150 mm focal length lenses would result in a total telescope length of 600 mm. By adding to this the approximate dimensions of the other components (PM, collimator and grating plus their mountings) the whole setup would be at least 800 mm in overall length, which is undesirable when considering, for instance, storage or transportation. The overall telescope length was therefore restricted to a maximum of 350 mm, which reduced the 7 pairs down to just 3. Table 1 shows the three possible lens combinations for the two collimators and the final beam widths they produce.

F240APC-C (W_0 = 1.5 mm)			**F280APC-C (W_0 = 3.4 mm)**		
Lens Combination (f_1xf_2)	Overall Length (mm)	Final Beam Diameter W_2 (mm)	Lens Combination (f_1xf_2)	Overall Length (mm)	Final Beam Diameter W_2 (mm)
75x100	350	2.03	60x35	190	2.05
40x60	200	2.33	60x40	200	2.34
75x60	270	1.24	100x35	270	1.23

Table 1. The final three lens combinations for each of the two collimators. All possible combinations were considered but filtered down to just three after the criteria was met to ensure that the final beam width W_2 is smaller than the visible facet width. The Overall Length is equal to the total length of the telescope, $2(f_1+f_2)$. Matching pairs of beam widths were allowed up to a $\pm 30\,\mu m$ difference between their values when making a selection for comparison.

Only the first pair in this table (top row) has been compared experimentally and reported in this paper; however we can draw the early conclusion that, despite many possible combinations existing for just six different focal lengths, only a small selection of these combinations will be suitable for our PM. Clearly care must be taken when choosing the focal lengths to avoid vignetting and therefore losing power.

Two cage assemblies were built to accommodate the telescopes for each of the lens combinations. The spectral filter in each case was carefully adjusted to provide optimum performance. This was achieved by inserting the output fibre of the spectral filter into a spectrum analyser and adjusting the various degrees of motion until the power output and bandwidth had been maximised, ensuring the correct central wavelength was selected.

Once the alignment was optimised, the spectral filter was connected to a fibre based interferometer array with free space, fibre-to-fibre reference arm and an object arm consisting of a collimator and a retroreflector mirror. A balanced detector and an oscilloscope were used to measure the intensity of the interference signal as the optical path difference (OPD) was changed by 50 µm increments, 3 mm either side of zero OPD, over a total range of 6 mm. A fast Fourier transform of the signal was taken on the oscilloscope to measure the interference signal intensity and the frequency of the fringe spacing.

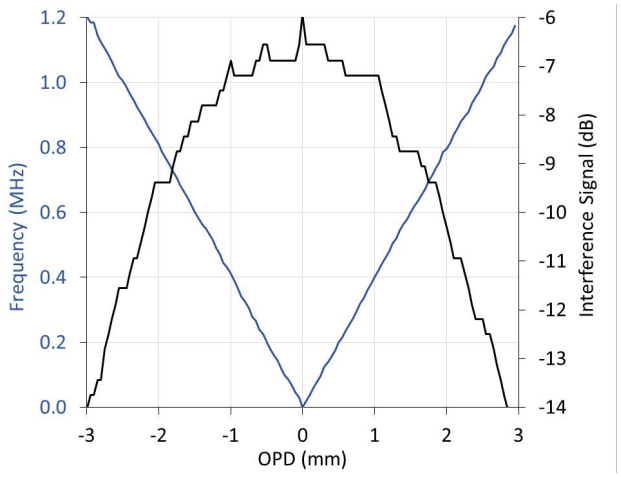

Figure. 3 a) F240APC-C 1.5 mm collimator, 70x100 mm focal lengths. The signal falls rapidly over the 3 mm displacement. Average signal drop-off is 2.67 dB/mm (black curve).

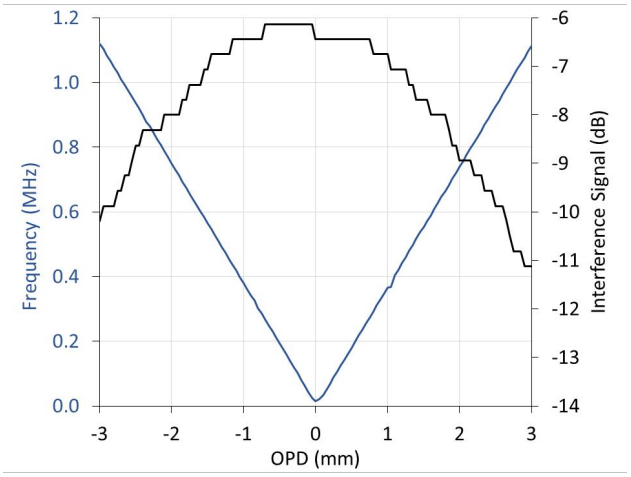

Figure. 3 b) F280APC-C 3.4 mm collimator, 60x35 mm focal lengths. The signal falls less rapidly over the 3 mm displacement. Average signal drop-off is 1.67 dB/mm (black curve).

The results indicate that a stronger signal is received by the detector for the setup using the 3.4 mm collimator, whereby less of the signal is lost over a 3 mm displacement. There is an average drop-off of approximately 2.67 dB/mm for the 1.5 mm collimator and 1.67 dB/mm for the 3.4 mm collimator. The larger beam width and shorter focal lengths have resulted in an average power improvement of 32.5%.

The shorter focal lengths have also reduced the effect of aberration by forcing the beams to propagate closer to the centre of the lenses (paraxial propagation). In the first arrangement, using f_1 = 75 mm, the spectrum was distributed over a larger surface area on Lens 1. Whereas in the second arrangement, using f_1 = 60 mm, the distance to Lens 1 is shorter, meaning that the spectrum is not given the opportunity to diverge as much as the first. The shorter distance from the grating to Lens 1 projects the spectrum over a smaller surface area of Lens 1 and therefore the marginal rays refract less and experience less aberration.

A shorter focal length illuminates a smaller area on the surface of Lens 1, which translates through to Lens 2. This directly impacts the converging angle on the PM depending on the focal lengths being used. If a shorter focal length is used on Lens 1, a shorter focal length on Lens 2 can also be used, which will reduce the overall length of the telescope and therefore the overall footprint of the spectral filter, although this could be detrimental to the total accepted bandwidth if care is not taken to ensure that the converging angle is equal-to-or-less-than the acceptance angle of the PM.

The approximate angular displacement of the converging angle for each setup can be calculated using the ratio of their numerical apertures and the focal lengths of the telescope, $NA_2 = NA_1(f_2/f_1)$. Since we already know $NA_1 = 11.78°$, the 1.5 mm collimator, using the longer focal length $f_2 = 100$ mm, results in a converging angle of 8.84° while the 3.4 mm collimator, using the shorter focal length $f_2 = 35$ mm, results in a converging angle of 20.19°, which is more than double the acceptance angle of the PM (10°). Therefore, finer linewidths have been produced for the 3.4 mm collimator at the cost of filtering a much narrower central portion of the total bandwidth whereby the marginal wavelengths from the edges of the converging spectrum have been left unfiltered. Approximately 50% of the total input bandwidth has been lost due to the increased size of the converging angle. This restricts the minimum and maximum tuned wavelengths to approximately 1303 nm and 1359 nm respectively.

4. CONCLUSIONS

This study has highlighted the impact of selecting the correct lenses to use in a free space PM-based spectral filter for SS-OCT. The bandwidth reduction experienced when chosen incorrectly has a greater impact on the performance than any other parameter, whereby 50% of the input spectrum may be lost due to incorrectly matching the converging angle of the telescope to the acceptance angle of the PM.

The second collimator with the 3.4 mm beam width was successful at improving the output signal strength and suffered from less aberrations but at the cost of reducing the successfully tuned portion of the spectrum. This was caused by the focal length of Lens 2, which increased the converging angle to over two times the acceptance angle of the PM. However, this did have the positive effect of reducing the instantaneous linewidths. For SS-OCT imaging, this would improve the penetration depth but decrease the resolution, whereas in general the inverse is considered more preferable.

A reduced effect from aberration is highly desirable in this type of setup since it ensures that higher power transmission is achieved and that only the smallest linewidths are recaptured by the collimator. Stray wavelengths from neighbouring portions of the spectrum may re-enter the fibre if the effects of aberrations are large. This study prompts the question of whether larger diameter lenses may have a role to play in reducing aberrations and therefore achieve finer tuning.

Future work also includes other configurations of PM-based SSs, including telescope-less ones[12].

ACKNOWLEDGMENTS

Mike Everson would like to thank the Engineering and Physical Sciences Research Council (EPSRC) for funding the project. George Dobre and Virgil-Florin Duma acknowledge the support of the Romanian National Authority for Scientific Research, CNDI–UEFISCDI project PN-III-P2-2.1-PED-2016-1937 (http://3om-group-optomechatronics.ro/).

REFERENCES

[1] Fan, J., Wang, P., Gao, F., Hu, Z., Kong, W., Li, H., & Shi, G. “Phase and amplitude correction in polygon tunable laser-based optical coherence tomography,” J. Biomed. Opt, 22(9), 096013 (2017).

[2] Bräuer, B., Lippok, N., Murdoch, S. G., Vanholsbeeck, F., “Simple and versatile long range swept source for optical coherence tomography applications,” J. Opt. 17(12), 125301 (2015).

[3] Motaghiannezam, S. R., Koos, D., and Fraser, S. E., “Differential phase-contrast, swept-source optical coherence tomography at 1060 nm for in vivo human retinal and choroidal vasculature visualization,” J. Biomed. Opt, 17(2), 0260111-0260115 (2012).

[4] Lee, K. K., Mariampillai, A., Joe, X. Z., Cadotte, D. W., Wilson, B. C., Standish, B. A., and Yang, V. X., “Real-time speckle variance swept-source optical coherence tomography using a graphics processing unit,” Biomed. Opt. Express 3(7), 1557-1564 (2012).

[5] Leung, M. K., Mariampillai, A., Standish, B. A., Lee, K. K., Munce, N. R., Vitkin, I. A., & Yang, V. X., “High-power wavelength-swept laser in Littman telescope-less polygon filter and dual-amplifier configuration for multichannel optical coherence tomography,” Optics letters, 34(18), 2814-2816 (2009).

[6] Johnson, B., Atia, W., Kuznetsov, M., Goldberg, B. D., Whitney, P., Flanders, D. C., "Analysis of a spinning polygon wavelength swept laser," arXiv preprint arXiv:1501.07003 (2015).
[7] Mao, Y., Flueraru, C., Sherif, S., & Chang, S., "High performance wavelength-swept laser with mode-locking technique for optical coherence tomography," Opt. Commun., *282*(1), 88-92 (2009).
[8] Wieser, W., Klein, T., Draxinger, W., and Huber, R., "Fully automated 1.5 MHz FDML laser with 100 mW output power at 1310 nm," European Conference on Biomedical Optics Optical Society of America, p. 954116, (2015).
[9] Oh, W. Y., Vakoc, B. J., Shishkov, M., Tearney, G. J., & Bouma, B. E., ">400 kHz repetition rate wavelength-swept laser and application to high-speed optical frequency domain imaging," Opt. Lett., 35(17), 2919-2921 (2010).
[10] Leung, M. K., Mariampillai, A., Standish, B. A., Lee, K. K., Vitkin, I. A., and Yang, V. X., "Simultaneous 6-channel optical coherence tomography using a high-power telescope-less polygon-based swept laser in dual-amplifier configuration," Proc. SPIE,.7554, 755418-755418 (2010).
[11] Oh, W. Y., Yun, S. H., Tearney, G. J., and Bouma, B. E., "115 kHz tuning repetition rate ultrahigh-speed wavelength-swept semiconductor laser," Opt. Lett., 30(23), 3159-3161 (2005).
[12] Duma, V.-F. and Podoleanu, A. Gh., "Polygon mirror scanners in biomedical imaging: a review," Proc. SPIE 8621, 8621V (2013).